Multi-particle collision dynamics simulations of sedimenting colloidal dispersions in confinement

Adam Wysocki,*[a] C. Patrick Royall,[bd] Roland G. Winkler,[c] Gerhard Gompper,[c] Hajime Tanaka,[d] Alfons van Blaaderen[e] and Hartmut Löwen*[a]

Received 26th January 2009, Accepted 6th March 2009
First published as an Advance Article on the web 2nd September 2009
DOI: 10.1039/b901640f

The sedimentation of an initially inhomogeneous distribution of hard-sphere colloids confined in a slit is simulated using the multi-particle collision dynamics scheme which takes into account hydrodynamic interactions mediated by the solvent. This system is an example for soft matter driven out of equilibrium where various length and time scales are involved. The initial laterally homogeneous density profiles exhibit a hydrodynamic Rayleigh–Taylor-like instability. Solvent backflow effects lead to an intricate non-linear behaviour which is analyzed via the solvent flow field and the colloidal velocity correlation function. Our simulation data are in good agreement with real-space microscopy experiments.

1 Introduction

Mesoscopic colloidal dispersions embedded in a molecular solvent are soft matter systems which need multiscale modelling. For structural equilibrium correlations, this is mainly a problem of different length scales which has been widely addressed and is by now well-understood, *e.g.* by using the concept of effective interactions.[1] For dynamical correlations and non-equilibrium situations, widely different time scales require careful multiscale modelling. The dynamics of a molecular solvent takes place on the picosecond level, while the time a colloid needs to diffuse over its own radius, is in the second time scale for micron-sized colloids. The hydrodynamic interactions[2] between the colloidal particles are mediated by the solvent flow on an intermediate time scale and are long-ranged and of many-body nature. It is only at very low colloidal volume fractions that hydrodynamic interactions can be neglected. Recently, various computational schemes have been developed to tackle hydrodynamic interactions ranging from the lattice Boltzmann technique,[3] fluidized particle methods[4] to multi-particle collision dynamics (MPCD)[5–7] where the solvent flow is modelled as ideal gas particles which exchange momentum locally by stochastic rotation of the relative velocities.

[a]*Institut für Theoretische Physik II, Heinrich-Heine-Universität Düsseldorf, Universitätsstrasse 1, D-40225 Düsseldorf, Germany. E-mail: adam@thphy.uni-duesseldorf.de; hlowen@thphy.uni-duesseldorf.de*
[b]*School of Chemistry, University of Bristol, Bristol, BS8 1TS, UK*
[c]*Institut für Festkörperforschung, Forschungzentrum Jülich, D-52425 Jülich, Germany*
[d]*Institute of Industrial Science, University of Tokyo, 4-6-1 Komaba, Meguro-ku, Tokyo, 153-8505, Japan*
[e]*Soft Condensed Matter Group, Debye Institute for Nanomaterials Science, Utrecht University, PO Box 80000, 3508, TAUtrecht, The Netherlands*

Here we consider a hydrodynamic instability of sterically-stabilized colloids (hard spheres) confined to a slit by inverting gravity which acts perpendicular to the slit. We simulate the hydrodynamic instability and incorporate the crucial hydrodynamic interactions by using the MPCD scheme.

The motion of a colloid is characterised by the Peclet number $Pe = \tau_D/\tau_S$, which is the ratio between the time τ_D it takes a particle to diffuse its own radius and the time τ_S it takes to sediment the same distance. A Peclet number of order unity is the dividing line between colloidal ($Pe \leq 1$) and granular systems ($Pe \gg 1$), *i.e. Pe* measures the importance of Brownian motion. The classical Rayleigh–Taylor instability, which occurs if a heavy, immiscible fluid layer is placed on top of a lighter one has been intensively studied for the case of a simple Newtonian fluid both by theory,[8] simulation[9] and experiment, and is observed in granular matter,[10–12] in surface-tension dominated colloid–polymer mixtures[13] and in a suspension of dielectric particles exposed to an ac electric field gradient.[14] However, except for ref. 15, this instability was never simulated on the particle scale in the context of colloidal sedimentation in confinement including hydrodynamic interactions. Here we present simulation data using the MPCD method. The instability is resolved on the colloidal particle scale and good agreement with real-space experiments is observed. We further show that the instability is accompanied by significant solvent backflow effects. Finally, correlations of the colloidal velocities are calculated which reveal strong lateral correlations and anticorrelations which are time-dependent.

The paper is organized as follows: in chapter II the simulation method is briefly described. Results for the sedimentation problem are presented in chapter III and compared to real-space confocal microscopy data. The instability and the concomitant solvent flow fields and colloidal velocity correlations are discussed. Finally, we present our conclusions in chapter IV.

2 The simulation model

Our model consists of a suspension of N solute particles with mass M and hard sphere diameter σ immersed in a bath of N_s solvent particles with mass m and a number density $N_s = N_s/V$, here V is the volume of the simulation box. The system is confined between two walls with distance L in x-direction and has periodic boundary conditions otherwise. The N colloidal particles with space position $\mathbf{R}_i$ and velocity $\mathbf{V}_i$ propagate according to Newton's equation of motion

$$M\frac{\mathrm{d}\mathbf{V}_i}{\mathrm{d}t} = F_S\mathbf{e}_x - \sum_{j\neq i}\nabla_{\mathbf{R}_j}V(R_{ij}) + F_w(X_i)\mathbf{e}_x$$

The first term on the right hand side is the constant driving force of strength F_S directed perpendicular to the walls in the x-direction and the second one represents the force due to the interaction with other colloids ($R_{ij} = |\mathbf{R}_i - \mathbf{R}_j|$ is the interparticle distance). The third term is a repulsive wall–colloid force. To avoid overlap the colloids interact *via* a screened Coulomb potential which diverges at $R_{ij} = \sigma$, here the reduced inverse screening length is $\kappa\sigma = 40$. A similar potential is used for the colloid–wall interaction. We integrate the equation of motion using a velocity Verlet algorithm with a time step δt. Simultaneously, the solvent particles with space position $\mathbf{r}_i$ and velocity $\mathbf{v}_i$ move ballistically also within the same time step δt, *i.e.*

$$\mathbf{r}_i(t + \delta t) = \mathbf{r}_i(t) + \mathbf{v}_i(t)\delta t \tag{2}$$

To enforce no-slip boundary conditions on the colloid surface a stochastic reflection method[16,17] is applied. If a solvent particle i hits a colloid it gets a new velocity $\mathbf{u}_i = \mathbf{u}_{n,i} + \mathbf{u}_{t,i}$ relative to the velocity of the colloids boundary from a distribution for the normal velocity component $P_n(u_n) = m\beta u_n e^{-m\beta u_n^2/2}$ and the tangential velocity

component $P_t(u_t) = \sqrt{m\beta/(2\pi)}e^{-m\beta u_t^2/2}$ with $\beta^{-1} = k_B T$. Then the new velocity of the solvent particle i after collision with the colloid j reads as

$$\mathbf{v}_i(t + \delta t) = \mathbf{V}_j(t) + \mathbf{\Omega}_j(t) \times (\tilde{\mathbf{r}}_i - \mathbf{R}_j(t)) + \mathbf{u}_i \tag{3}$$

where $\mathbf{\Omega}_j$ is the angular velocity of the colloid and $\tilde{\mathbf{r}}_i$ is the point of contact at the colloid surface. After all collisions within δt are completed, the new velocity of the colloid j is updated as

$$\mathbf{V}_j(t + \delta t) = \mathbf{V}_j(t) + \frac{m}{M}\sum_{i \in C}\big(\mathbf{v}_i(t) - \mathbf{v}_i(t + \delta t)\big) \tag{4}$$

and the new angular velocity is

$$\mathbf{\Omega}_j(t + \delta t) = \mathbf{\Omega}_j(t) + \frac{m}{I}\sum_{i \in C}\big(\tilde{\mathbf{r}}_i - \mathbf{R}_j(t)\big) \times \big(\mathbf{v}_i(t) - \mathbf{v}_i(t + \delta t)\big) \tag{5}$$

where C is the set of solvent particles colliding with colloid j in the time interval $[t, t + \delta t]$ and $I = 2/5M(\sigma/2)^2$ is the moment of inertia of the spherical colloids.

After a time $\Delta t = n\delta t$ the solvent particles interact with each other *via* a multi-particle collision.[5] The particles are sorted in cubic cells of size a and the center-of-mass velocity $\mathbf{U}_\xi = N_\xi^{-1}\sum_{j \in \xi}\mathbf{v}_j$ of each cell ξ is calculated (N_ξ is the number of particles in the cell ξ). Then in each cell the relative velocities $\delta\mathbf{v}_i = \mathbf{v}_i - \mathbf{U}_{\xi_i}$ are rotated by an angle α around a random axis, *i.e.*

$$\mathbf{v}_i(t + \Delta t) = \mathbf{U}_{\xi_i}(t) + S_{\xi_i}\hat{\omega}_{\xi_i}(\alpha)\delta\mathbf{v}_i(t) \tag{6}$$

where $\hat{\omega}_{\xi_i}(\alpha)$ is the stochastic rotation matrix and S_{ξ_i} is a thermostat operator (see below). $\hat{\omega}_{\xi_i}(\alpha)$ is equal for all particles within the same cell but uncorrelated between different cells and in time. Due to this operation the particles exchange momentum in the cell while the total kinetic energy and the total momentum in the cell are conserved. It was shown[5] that (2) and (6) lead in equilibrium to a Maxwell–Boltzmann distribution of the velocities and that Navier–Stokes-hydrodynamics is generated.

Since in any kind of a non-equilibrium simulation thermostating is required to avoid viscous heating, we rescale the relative velocities $\delta\mathbf{v}_i$ in each cell by a factor

$$S_\xi = \sqrt{\frac{3(N_\xi - 1)k_B T}{m\sum_{i \in \xi}\delta\mathbf{v}_i^2}} \tag{7}$$

This thermostat acts locally and is unbiased with respect to the flow field and hence does not destroy the hydrodynamic behaviour, see ref. 18.

For a small mean free path $\lambda = \Delta t\sqrt{k_B T/m} \ll a$ the same set of particles interact over several Δt with each other before leaving this cell and hence they remain correlated over several Δt. If one imposes a flow field the degree of correlation and therefore the transport coefficients depends on the magnitude of the flow field. The violated Galilean invariance can be restored if all particle positions are shifted by a random vector before the collision step.[19]

At the wall surfaces we also enforce no-slip boundary conditions using a stochastic reflection method but additionally we fill the wall cells with $n_s a^3 - N_\xi$ "ghost" particles during the collision step ($n_s a^3$ is the average number of solvent particles in the collision cell), because due to the random shift partially occupied boundary collision cells occur.[20] The velocities of the "ghost" particles are drawn from a Maxwell–Boltzmann distribution with zero mean and variance $k_B T$.

We employed the parameters $\Delta t = 0.2\tau$, $\alpha = 3\pi/4$, $n_s a^3 = 5$ with $\tau = \sqrt{ma^2/(k_B T)}$. With these parameters the total solvent kinematic viscosity is $\nu = \eta/\rho \approx 0.5a^2/\tau$

($\rho = mn_s$ is the mass density and η the dynamic viscosity).[21] For the colloids we use $M = 167m$, hard core diameter $\sigma = 4a$ and $\delta t = \Delta t/4$. We calculate the diffusion constant in a bulk simulation from the integral of the velocity autocorrelation function and obtain $D = 0.013a^2/t_0$.[17] With these parameters we achieve the hierarchy of time scales for a colloidal particle $\Delta t = 0.2\tau < \tau_c = 1.5\tau < \tau_B = 2.2\tau < \tau_\nu = 8\tau < \tau_D = 307\tau$, see ref. 22. Here τ_c is the time a sound wave needs to propagate over one colloidal radius (the speed of sound is $c = \sqrt{5k_BT/(3m)}$), τ_B is the time the velocity of a colloid is correlated and τ_ν is the time over which the solvent momentum diffuses over one colloidal radius. We performed simulations up to $Pe_{max} = 4.8$ which correspond to a maximal Reynolds number of $Re_{max} = D/\nu Pe_{max} \approx 0.125 < 1$, such that inertial effects are negligible. To avoid compressibility effects we also ensure that the Mach number is smaller than unity, $Ma_{max} = 2D/(\sigma c)Pe_{max} = 0.024 \ll 1$. With these values of the hydrodynamic numbers and the hierarchy of time scales we are sure that a comparison with a real physical system is reasonable.

The system we consider contains $N = 15\,048$ hard sphere particles and $N_s = 14\,274\,843$ solvent particles in a box of $L/\sigma = 18$ and $L_y/\sigma = L_z/\sigma = 54$. We start our simulation with a fully equilibrated system under the influence of a constant force in the x-direction, *i.e.* particles have collected and settled at the top of the box. Then at time $t = 0$ we instantaneously reverse the direction of the force and monitor the evolution of the system until all particles have sedimented to the bottom.

We compare our simulation to single-particle level confocal microscopy experiments with sterically stabilised polymethylmethacrylate colloids. The value of the Peclet number can be adjusted by variation of the density mismatch between colloid and solvent mass density. Prior equilibration was achieved by placing the suspension overnight such that it sedimented across a thin (typically 50 μm) capillary. The capillary was then inverted, and the evolution under sedimentation was followed. More details of the experiment are described in ref. 23,24.

3 Results

A situation where a layer of a heavy fluid is on top of a lighter one is clearly mechanically unstable, *i.e.* the system is inclined to invert. During this process the initially

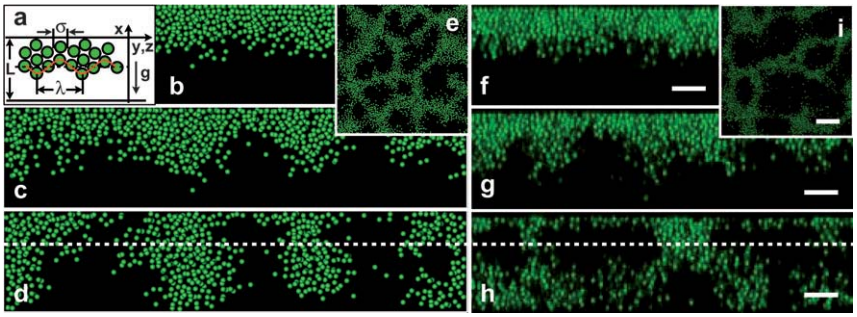

Fig. 1 Simulation and confocal microscopy snapshots. (a) A schematic illustrating the spatial parameters σ, λ and L. (b–e) Simulation snapshots of a system which contains $N = 33\,858$ colloidal particles and $N_s = 32\,118\,397$ solvent particles (not displayed) in a simulation box with dimensions $L/\sigma = 18$ and $L_y/\sigma = L_z/\sigma = 81$. The value of the Peclet number is $Pe = 1.6$. (b–d) Time series of the system at time $t/\tau_S = 3.2$ (b), 6.4 (c), 9.6 (d). The snapshots are slices of thickness 2σ done in the xy plane. (e) Slice of thickness 2σ in the yz plane at time $t/\tau_D = 9.6$. The height of the yz plane is $x/L = 2/3$, as indicated by the dashed line in (d). (f–i) Experimental realisation of the Rayleigh–Taylor-like instability in sedimentation of confined colloids. (f–h) Time series of images taken with a confocal microscope in the xy plane for the parameters $\phi = 0.15$, $Pe = 1.1$ and $L/\sigma = 18$ at times $t/\tau_S = 1.43$ (f), 5.5 (g), 11.22 (h). (i) Slice in the yz plane at a height $x/L = 2/3$ (indicated by the dashed line in (h)) at time $t/\tau_S = 11.22$. In (f–h) the scale bars denote 20 μm and in (i) 40 μm.

flat interface starts to develop perturbations with a characteristic wavelength $\lambda = 2\pi/k$, where k is a wave number.

We present snapshots of the time evolution of the system, in Fig. 1b–e from computer simulation, and in Fig. 1f–i from confocal microscopy. The similarity is remarkable, and we note that, at the very least, our simulation qualitatively reproduces the experiment. The time evolution in the development of the instability with a characteristic wavelength is clear. While snapshots in the gravity plane (Fig. 1b, c, d, f, g, and h) illustrate the overall process of sedimentation, snapshots in the horizontal yz plane show the transient pattern or network-like structure that results from the instability (Fig. 1e and i). At later times, the network structure decays and a laterally homogenous density profile develops where the colloids start to form a layer at the bottom of the cell which becomes more compact with time. In the initial regime of the instability, more precisely in a regime where the amplitude of an undulation is smaller than the corresponding wave length, the experimental and the simulation data are in line with the results of a linear stability analysis. A detailed comparison is presented in ref. 23 revealing a fastest growing mode with a wave number k_{max}.†

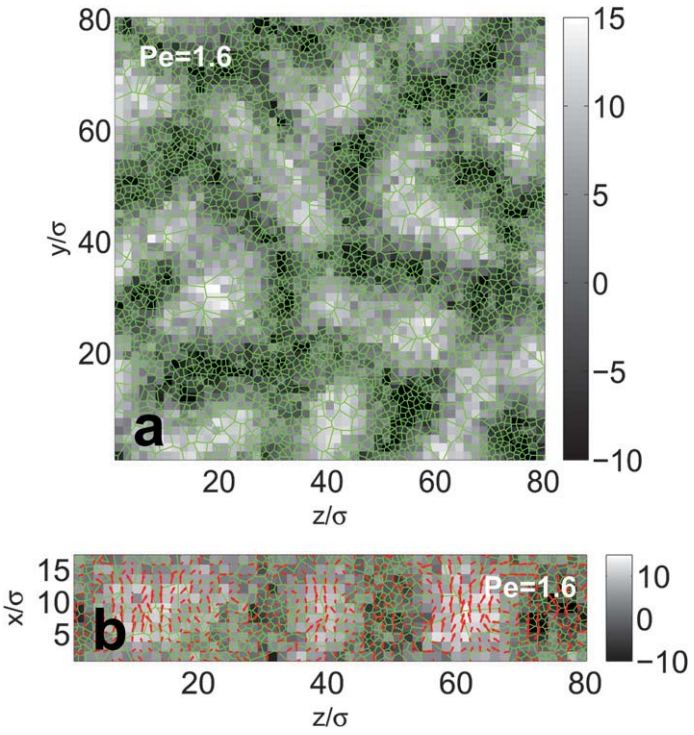

Fig. 2 Solvent flow field. (a) Solvent velocity field in the yz plane. Slice of the simulation box in the yz plane at a height $x/L = 1/2$ at time $t/\tau_S = 11.2$. The parameters are $Pe = 1.6$ and $L/\sigma = 18$. The colour plot represent the magnitude of the solvent velocity $v_x(y, z)/V_s$ in gravity direction, where V_s is the sedimentation velocity at infinite dilution. The Voronoi diagram of the colloid positions in this plane is indicated by green lines. (b) Solvent velocity field in the xz plane. Slice of the simulation box in the xz plane for the same parameters as in (a). The colour plot represent $v_x(x, z)/V_s$, the red arrows the velocity field $(\mathbf{v}_x + \mathbf{v}_z)(x,z)/V_s$ and the green lines the Voronoi diagram of the colloid positions in this plane.

† We remark that both the wave length and the growth rate of the most unstable undulation depends on the slit size L, more details on the slit size dependence are discussed in ref. 23.

Let us now study the solvent flow accompanying the colloidal instability. In Fig. 2 a, the solvent velocity field in the *yz* plane perpendicular to the driving force is shown at an intermediate height $x = L/2$. Inhomogeneities are revealed on the same length scale λ_{max} as in the colloidal density profile. Actually there is a back-flow effect associated with colloid-rich regions moving downwards and with solvent-rich regions of upward motion. This is clearly revealed in Fig. 2 b where a region rich in colloidal particles is shown as a dense Voronoi tesselation and clearly correlates with a downwards solvent velocity and *vice versa*. Again, the structures exhibit the characteristic length scale $\lambda_{max} = 2\pi/k_{max}$, the fastest growing wavelength in the linear regime.

We finally consider the spatial correlations of colloid-velocity fluctuations in the gravity direction in the plane perpendicular to gravity $C_x(x,r,t) = \langle \delta V_x(x,0,t)\delta V_x(x,r,t)\rangle$, where $\delta V_x(x,r,t) = \langle v_x(x,t)\rangle - v_x(x,r,t)$ are the deviations from the mean velocity in the *yz* plane at height x from distance r in this plane. We anticipate both positive correlations at short distances (within the same 'branch' of the network) and negative correlations at slightly longer length scales. At longer length scales again, the lack of long-ranged order in the network leads to a loss of correlation and a decay $\lim_{r \to \infty} C_x(x,r,t) = 0$. In Fig. 3 a–c the chronological development of the logarithm of the absolute value of $C_x(x, r, t)$ is shown at the height $x = L/2$ for $Pe = 0.8$, 1.6, 4.8, respectively. The maximum in anticorrelation of $C_x(x, r, t)$ is found at $r \approx \lambda_{max}/2$, see Fig. 3 d, in other words the length scale of the network

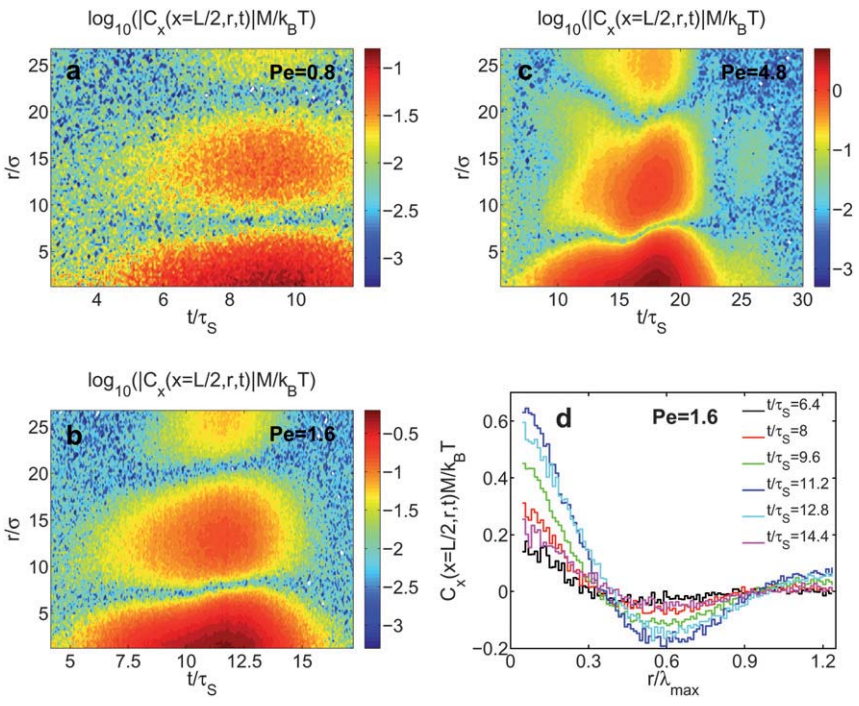

Fig. 3 Spatial correlation functions of the colloid velocity fluctuations. (a–d) The spatial correlation function. The spatial correlation function $C_x(x = L/2, r, t)$ of the colloid velocity fluctuations in the gravity field direction is measured as a function of the distance r perpendicular to gravity. $C_x(x = L/2, r, t)$ was obtained in the *yz* plane at $x/L = 1/2$ for $Pe = 0.8$ (a), $Pe = 1.6$ (b,d), $Pe = 4.8$ (c) and $L/\sigma = 18$. $C_x(r)$ is scaled by thermal fluctuation strength $k_B T/M$ (M is the colloid mass). In (a–c) r is scaled by the diameter σ of the colloidal particle and in (d) by the wave length λ_{max} of the fastest growing undulation for $Pe = 1.6$. The chronological development of the logarithm of the absolute value of $C_x(x = L/2, r, t)$ is shown in (a–c), whereas in (d) $C_x(x = L/2, r, t)$ is plotted for times $t/\tau_S = 6.4$, 8, 9.6, 11.2, 12.8, 14.4.

structure corresponds very closely to the fastest growing wavelength predicted by the linear stability analysis. The velocity correlations become more pronounced in the non-linear mixing regime which is an indication of fully developed swirls of solvent and particle-rich regions. For $Pe = 0.8$ (Fig. 3 a) and for $Pe = 1.6$ (Fig. 3 b,d) the correlation length slightly increases in time, while for $Pe = 4.8$ (Fig. 3 c) it is markedly *non-monotonic* in time revealing a non-trivial interplay between sedimentation, hydrodynamics and confinement.

4 Conclusions

Using the MPCD simulation technique, we have presented an analysis of a hydrodynamic instability in a colloidal system confined in a slit of micrometre dimensions. Our results show good agreement between experiment and simulation, showing that the latter accurately describes the fundamentally and practically important phenomena caused by hydrodynamic instabilities.

Let us finally discuss some possible extensions of the present work: here we started with a sedimentation density distribution, typical for an experimental situation before turning over the cell. A sharp initial interface as often encountered after flow junctions in microfluidics as well as a linear density gradient, as often found in systems with source–drain stabilized electrolyte concentrations could also be addressed in principle by simulation. We would expect that the instability is most pronounced for high initial density gradients.

Finally, it is tempting to consider more complex interactions between the colloidal particles as realized, for example, for colloid-polymer mixtures where strong attractions can be realized.‡ One would then expect a Rayleigh–Taylor-like instability with surface tension.[27] Also binary systems will establish a playground for sedimentation instabilities where separation and mixing could be tuned by the strength of the drive. External drives which are oscillatory in time could lead to segregation effects in the axial direction[28] and might be interesting for further study. If the initial density profile is crystalline in the lateral direction,[23] surface melting behaviour in non-equilibrium becomes relevant.[29] The recrystallization at the bottom of the cell[30] might be a complex process, in particular for attractive interactions and binary systems.

5 Acknowledgements

We thank T. Palberg for helpful discussions. This work was supported by the SFB TR6 (projects A3, A4 and D3). C. P. R. acknowledges the Royal Society for Funding. H. T. acknowledges a grant-in-aid from MEXT. We acknowledge ZIM for computing time.

References

1 J.-P. Hansen and H. Löwen, *Annu. Rev. Phys. Chem.*, 2000, **51**(1), 209–242.
2 J. K. G. Dhont, *An Introduction to the Dynamics of Colloids*, Elsevier, Amsterdam, 1996.
3 M. E. Cates, K. Stratford, R. Adhikari, P. Stansell, J.-C. Desplat, I. Pagonabarraga and A. J. Wagner, *J. Phys.: Condens. Matter*, 2004, **16**(38), S3903–S3915.
4 H. Tanaka and T. Araki, *Phys. Rev. Lett.*, 2000, **85**(6), 1338–1341.
5 A. Malevanets and R. Kapral, *J. Chem. Phys.*, 1999, **110**(17), 8605–8613.
6 R. Kapral, *Adv. Chem. Phys.*, 2008, **140**, 89–146.
7 G. Gompper, T. Ihle, D. Kroll and R. Winkler, *Adv. Polym. Sci.*, 2009, **221**, 1.

‡ Strong attractions in colloid–polymer mixtures are responsible for a ultralow surface tension and hence for capillary waves.[25] Such long-wavelength interface roughness should enhance the initial growth of the unstable undulations as compared to a fully flat interface. On the other hand it was shown that the non-linear regime is not influenced much by the initial conditions.[26]

8 S. Chandrasekhar, *Hydrodynamic and Hydromagnetic Stability*, Oxford University Press, Oxford, 1961.
9 K. Kadau, T. C. Germann, N. G. Hadjiconstantinou, P. S. Lomdahl, G. Dimonte, B. L. Holian and B. J. Alder, *Proc. Natl. Acad. Sci. U. S. A.*, 2004, **101**(16), 5851–5855.
10 C. Völtz, W. Pesch and I. Rehberg, *Phys. Rev. E*, 2001, **65**(1), 011404.
11 J. L. Vinningland, Ø. Johnsen, E. G. Flekkøy, R. Toussaint and K. J. Måløy, *Phys. Rev. Lett.*, 2007, **99**(4), 048001.
12 E. Kuusela, J. M. Lahtinen and T. Ala-Nissila, *Phys. Rev. E*, 2004, **69**(6), 066310.
13 D. G. A. L. Aarts, R. P. A. Dullens and H. N. W. Lekkerkerker, *New J. Phys.*, 2005, **7**, 40.
14 J. Zhao, D. Vollmer, H.-J. Butt and G. K. Auernhammer, *J. Phys.: Condens. Matter*, 2008, **20**(40), 404212.
15 J. T. Padding and A. A. Louis, *Phys. Rev. E*, 2008, **77**(1), 011402.
16 Y. Inoue, Y. Chen and H. Ohashi, *J. Stat. Phys.*, 2002, **107**(1), 85–100.
17 J. T. Padding, A. Wysocki, H. Löwen and A. A. Louis, *J. Phys.: Condens. Matter*, 2005, **17**(45), S3393–S3399.
18 D. J. Evans and G. P. Morriss, *Phys. Rev. Lett.*, 1986, **56**(20), 2172–2175.
19 T. Ihle and D. M. Kroll, *Phys. Rev. E*, 2001, **63**(2), 020201.
20 A. Lamura, G. Gompper, T. Ihle and D. M. Kroll, *Europhys. Lett.*, 2001, **56**(3), 319–325.
21 N. Kikuchi, C. M. Pooley, J. F. Ryder and J. M. Yeomans, *J. Chem. Phys.*, 2003, **119**(12), 6388–6395.
22 J. T. Padding and A. A. Louis, *Phys. Rev. E*, 2006, **74**(3), 031402.
23 A. Wysocki, C. P. Royall, R. G. Winkler, G. Gompper, H. Tanaka, A. van Blaaderen and H. Löwen, *Soft Matter*, 2009, **5**, 1340–1344.
24 C. P. Royall, J. Dzubiella, M. Schmidt and A. van Blaaderen, *Phys. Rev. Lett.*, 2007, **98**(18), 188304.
25 D. G. A. L. Aarts, M. Schmidt and H. N. W. Lekkerkerker, *Science*, 2004, **304**(5672), 847–850.
26 K. Kadau, C. Rosenblatt, J. L. Barber, T. C. Germann, Z. Huang, P. Carlès and B. J. Alder, *Proc. Natl. Acad. Sci. U. S. A.*, 2007, **104**(19), 7741–7745.
27 A. Wysocki and H. Löwen, *J. Phys.: Condens. Matter*, 2004, **16**(41), 7209–7224.
28 A. Wysocki and H. Löwen, *Phys. Rev. E*, 2009, **79**(4), 041408.
29 H. Löwen and R. Lipowsky, *Phys. Rev. B*, 1991, **43**(4), 3507–3513.
30 T. Biben, R. Ohnesorge and H. Löwen, *Europhys. Lett.*, 1994, **28**(9), 665–670.

